Proxy-Based Sliding Mode Stabilization of a Two-Axis Gimbaled Platform

Özgür Hastürk, Aydan M. Erkmen, İsmet Erkmen

Abstract— **Nowadays, high portion of tactical missiles use gimbaled seekers. For accurate target tracking, the platform where the gimbal is mounted must be stabilized with respect to the motion of the missile body. Line of sight stabilization is critical for fast and precise tracking and alignment. Although conventional PID framework solves many stabilization problems, it is reported that many PID feedback loops are poorly tuned. In this paper, a recently introduced approach, proxy-based sliding mode control to a line-of-sight stabilization of two-axis gimbal system, is implemented. The tracking performance and disturbance rejection capability of the proxy-based sliding mode control is compared with that of conventional PID control. Simulation and experimental results both indicate clear superiority of the proxy-based sliding control performance.**

Index Terms— **Line-of-sight stabilization, Unscented Kalman Filter, PID control, proxy-based sliding mode control.**

I. Introduction

State-of-the-art missile systems use gimbaled electro-optical (EO) and infrared (IR) guidance systems because of excellent lethality of records and ease of operation. The principle that gimbaled guidance systems use to precisely stabilize optical line of sight (LOS) between target and seeker, even under vibrations and uncertainties caused by imprecisely estimated missile dynamics and aerodynamics [1,2], requires high-precision servo performance in order to provide a stabilized target image and high disturbance rejection to maintain the LOS to a target [3,4].

Disturbances that affect the line of sight are mainly due to missile angular motion or maneuvers, and air-stream induced torque. In addition, missile linear motion and vibration generate disturbance torques due to mass imbalance and gimbal geometry. Conventional LOS stabilization techniques employ rate gyros, or in general, rate sensors to sense the rate disturbances about the LOS. Controlling the gimbal system by using direct drive DC motor keeps LOS of the imaging sensor stabilized, but within unpredictable error bounds, since, in such systems, friction on mechanical bearings and the nonlinearities in system dynamics frequently cause stabilization error. Hence, LOS stabilization becomes a complicated task to be executed under uncertain disturbances due to not only uncertainties and nonlinearities of the controlled system but also to changes in the operating environment.

Gimbal stabilization controllers generally use classical PID. Although the PID framework solves many control problems and is sufficiently flexible to incorporate additional capabilities, it is reported that many PID feedback loops are poorly adjusted. In addition, these control strategies are known to lack adaptivity and robustness against changes in the operation environment [5, 6].

In the literature, several improvements to PID controllers are provided (for instance, see [7, 8]). For example, in order to decrease accumulating integration error, which causes actuator saturation, self–adjusting integral action is developed. In these approaches, experimental results illustrate that this self-tuning method yields higher precision and perfect control performance under linearity; however, serious disadvantages exist since nonlinear distortion destructs stability in such systems [8].

One of the alternatives to PID control is LQG/LTR control. LQG/LTR theory, developed from LQG optimal control theory, is a very effective design tool for linear multivariable feedback systems, where loop shapes of optimal full-state regulators or filters are approximated at plant inputs or outputs via certain specific choices of free parameters [6, 9]. However, uncertain system parameters must be identified and the magnitude of uncertainty should be known or estimated because LQG/LTR system may exhibit worse robustness qualities than the original LQG system [10].

In addition to these control techniques, many researchers have worked on stabilization of the gimbal with more advanced approaches, such as fuzzy logic and neural networks.

Fuzzy logic is widely used to solve problems with uncertainties and nonlinearities without a mathematical model and it provides certain level of intelligence to the conventional PID controllers, enabling them self-tuning ability and online adaptation. However, the fundamental problem is how to derive the required control rules upon which the success of the fuzzy control depends, because it is difficult to estimate the membership function [11, 12].

Neural networks have been utilized in nonlinear systems due to its ability to learn and handle nonlinearities and uncertainties present in the control system. The most useful property of neural networks is their ability to approximate arbitrary linear or nonlinear mapping through learning. However, gradient-based back propagation learning algorithms and real-time recurrent learning are major drawbacks of the neural network [13]. Gradient-based back

Manuscript received June 11, 2011 reviewed August 2, 2011.

Özgür Hastürk is with Roketsan Missiles Industries Inc., Ankara Samsun Karayolu 40. Km 06780 Ankara Turkey (phone: 0090-312-863-42-00; fax: 0090-312-863-42-08; (e-mail: ohasturk@roketsan.com.tr)

Aydan M. Erkmen is with Middle East Technical University, Dept. of Electrical and Electronics Engineering 06531 Ankara Turkey. (E-mail: aydan@metu.edu.tr).

İsmet Erkmen is with Middle East Technical University, Dept. of Electrical and Electronics Engineering 06531 Ankara Turkey. (E-mail: erkmen@metu.edu.tr).

ISBN: 978-988-18210-9-6
ISSN: 2078-0958 (Print); ISSN: 2078-0966 (Online)

propagation algorithm is simple and requires smaller amount of storage, however, it converges very slowly and the learning parameter which is experimentally assigned affects heavily the learning performance [14]. In addition, choosing the architecture of a neural network for a particular problem usually requires some prior knowledge of the problem's complexity and usually involves much trial and error [15].

Sliding mode control, on the other hand, is another popular control strategy dealing with nonlinear uncertain systems that avoids the abovementioned problems [16]. Sliding mode is often used to cope with any worst-case scenario resulting from interval bounded parametric perturbations, external disturbances and slip-stick friction. In addition, it provides robustness to the system and does not require perfect mathematical model in developing the controller [17]. However, repetition of delayed switching on the sliding surface causes high-frequency oscillations when sliding mode control is directly implemented as a real-time discrete controller.

Moreover, Proxy-based Sliding Mode Control (PBSMC), as introduced by Kikuuwe and Fujimoto in 2006 for robot control, combines accurate tracking and smooth response [18]. It produces slow, overdamped motion after actuator saturation without sacrificing accurate, responsive tracking capability during normal operations. It also can make the system behave compliantly to external disturbances. PBSMC is defined as a modified version of sliding mode control adapted to discrete environment and, at the same time, as an extension of force-limited PID control [18, 19].

In this paper, joint space version of PBSMC is adopted for LOS stabilization of a two-axis gimbaled system while the task-space version of PBSMC was introduced by Kikuuwe and Fujimoto in 2006. This task space is limited to 1-D PBSMC, which can be used for decentralized joint-angle control. Although, multidimensional PBSMC for task-space position control is empirically demonstrated as in [18, 19, 20], the joint-space velocity control implementation is not available. The proposed method is shown to possess good tracking performance and achieve smooth, almost critically damped, motion, both in simulations as well as on our actual experimental guidance platform.

The rest of this paper is organized as follows. Section II introduces the hardware on which the proposed stabilization methodology is implemented, and also derives the mathematical model of the LOS system. Section III is devoted to the proposed stabilization method based on PBSMC. Section IV presents the simulation results, analyzing the sensitivity of the method to parameter changes. Section V discusses the demonstrative results of the proposed approach on the actual hardware, while Section VI provides concluding remarks.

II. Experimental Setup

A. Hardware Description

The two-axis gimbaled system on which the experiments are conducted is illustrated in Fig. 1. This system has two actuators, which are brush-type direct drive DC motors, where each of their shafts is equipped with a low-resolution optical incremental encoder for measuring angular displacement. In addition, this setup has a two-axis MEMS rate sensor mounted on the inner gimbal to sense the disturbance about the LOS. The position and velocity of the gimbal are measured with incremental encoders and two-axis MEMS rate sensor, respectively. Since the stabilization controller is designed for steady guidance of missile to be launched from the platform, the base of the gimbaled platform is actuated in the azimuth axis by Newport XPS Controller to induce the required disturbance at the base of the gimbaled platform, in a way similar to real-life terrain navigation applications. The base motion of the gimbal system is measured with a miniature IMU.

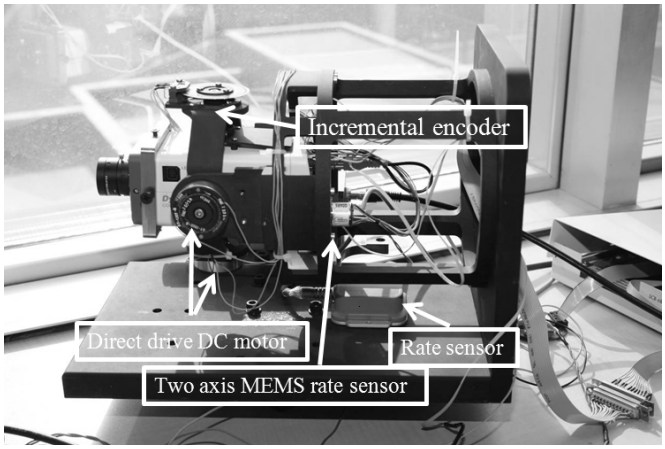

Fig. 1. Hardware – two-axis gimbaled system platform.

Fig. 2 shows the schematic representation of the whole hardware experimental setup, which is mainly composed of three parts: the plant representing our two-axis gimbaled platform of Fig.1, the controller, and the rate sensor filtering. The modeling of the two-axis gimbaled system is presented in the subsequent subsection.

Since our experimental setup includes a MEMS rate sensor, which has significant bias and random error values due to the limitation of the manufacturing technology, Unscented Kalman Filter (UKF) algorithm is used in rate sensor filtering in order to reduce the effect of uncertainty in the sensor state. The UKF algorithm, used for estimating the states of the rate sensor in the system, consists of sampling particles, prediction equations and updating equations. The sampling principle assumes that the state of the rate sensor has Gaussian distribution and sampling particles is calculated by fully matching the mean and covariance of the state variable if two moments of a random variable are available [21]. The prediction part of UKF computes the mean and covariance of the sigma points of the state by propagating them through the dynamic model and adds the process noise covariance to state covariance. The design of noise covariance matrix has proven to play an important role in improving the stability of the algorithm as also stated in [22]. Update algorithm of the UKF forms sigma points of the predicted state as in [23] and uses computational rules of Gaussian distributions for conditioning the joint distribution to the measurement after unscented transformation of the joint distribution of predicted state and measurement.

B. Mathematical Modeling

As seen in the block diagram of Fig. 2, the mathematical model of our experimental setup needs to be derived in order to design and justify operation of stabilization module in a simulation environment prior to its tests on the physical

ISBN: 978-988-18210-9-6
ISSN: 2078-0958 (Print); ISSN: 2078-0966 (Online)

hardware system. The nonlinear gimbal dynamical equations are derived using Lagrangian mechanics [24, 25].

The gimbal as seen in our platform is a pivoted support which allows the rotation of the imaging system about the elevation and the azimuth axes, as shown in Fig. 3, where φ is the azimuth angle and θ is the elevation angle of the payload with respect to base, which are controlled with a two-axis gimbaled mechanism.

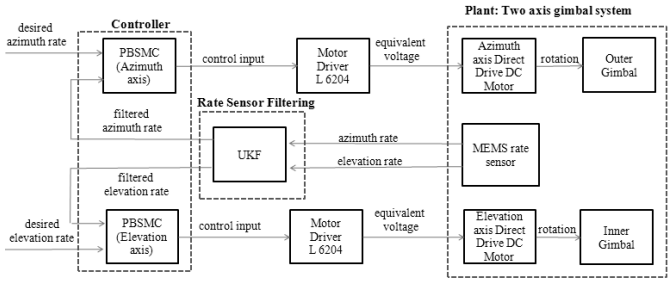

Fig. 2. Experimental setup – two-axis gimbaled system.

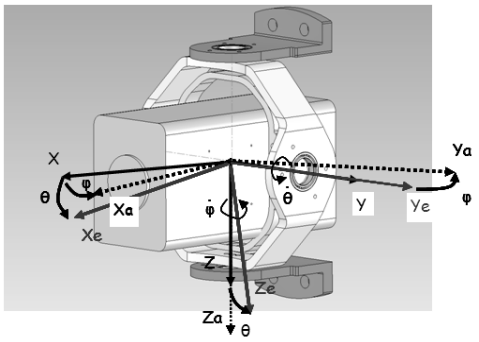

Fig. 3. Typical two axis gimbal system.

The equations of motion of such system can be derived directly from the Lagrangian, L=*T*-*V*. The kinetic (*T*) and the potential (*V*) energies of the system are, respectively,

$$T = \frac{1}{2}\left[(J_{Py} + J_{Iy})\dot{\theta}^2 + (J_{Pz} + J_{Iz})\dot{\phi}^2 \sin^2(\theta) + (J_{Px} + J_{Ix})\dot{\phi}^2 \cos^2(\theta) + (J_{Oz})\dot{\phi}^2\right] \quad (1)$$

and

$$V = mgl(\cos(\theta) - 1) \quad (2)$$

Here, the moment of inertia of the inner gimbal about the *X*, *Y* and *Z* axes are denoted as J_{Ix}, J_{Iy} and J_{Iz}, respectively. The moment of inertia of the payload about the *X*, *Y* and *Z* axes are represented as J_{Px}, J_{Py} and J_{Pz}, respectively. J_{Oz} represents the moment of inertia of the outer gimbal about the *Z* axis. In addition, *m* is the total mass of payload + inner gimbal, and *l* is eccentricity.

The corresponding Lagrange equations of the system are obtained as,

$$N_\phi = \frac{d}{dt}\left(\frac{\partial L}{\partial \dot{\phi}}\right) - \frac{\partial L}{\partial \phi} \quad (3)$$

$$N_\phi = (J_{Pz} + J_{Iz})(\ddot{\phi}\ \sin^2(\theta) + 2\dot{\phi}\,\dot{\theta}\ \sin(\theta)\cos(\theta)) + (J_{Px} + J_{Ix})(\ddot{\phi}\ \cos^2(\theta) - 2\dot{\phi}\dot{\theta}\ \sin(\theta)\cos(\theta)) + J_{Oz}\ddot{\phi} \quad (4)$$

$$N_\theta = \frac{d}{dt}\left(\frac{\partial L}{\partial \dot{\theta}}\right) - \frac{\partial L}{\partial \theta} \quad (5)$$

$$N_\theta = (J_{Py} + J_{Iy})\ddot{\theta} + (J_{Px} + J_{Ix} - J_{Pz} - J_{Iz})\dot{\phi}^2 \cos(\theta)\sin(\theta) + \frac{1}{2}mgl\sin(\theta) \quad (6)$$

where N_θ and N_φ are the corresponding generalized forces, which in this case turn out to be the torques.

III. Proxy Based Sliding Mode Control (PBSMC)

PBSMC is a new control scheme, first introduced by Kikuuwe and Fujimoto in [18]. The idea behind PBSMC is to attach a virtual object referred as a proxy through a virtual coupling controlled object. The virtual coupling can perform PID-type control action to maintain its length as zero. This method is adopted and implemented for the inner gimbal of the platform, which is illustrated in Fig. 4, and in 2D for ease of understanding. Here the proxy depicted as constrained virtual surfaces is a mass connected to the inner gimbal by a PID type virtual coupling. The position of the proxy is controlled via sliding mode control that exerts a control torque $T_{\theta p}$. The proxy also accepts forces from a PID-type virtual coupling that causes a counter torque T_θ between proxy and inner gimbal. The classically known sliding mode control law to control the proxy is used and formulated as

$$T_{\theta p} = U\,\mathrm{sgn}(S) \quad (7)$$

Here, *U* is the control gain that varies each step *k* and *S* is the sliding surface, which uses the dynamic approach error vector:

$$S = (q_d - q_p) + \lambda(\dot{q}_d - \dot{q}_p) \quad (8)$$

where q_p and $\dot{q}_p$ are position and velocity of the proxy, respectively, and q_d and $\dot{q}_d$ are the desired position and velocity of the inner gimbal, respectively.

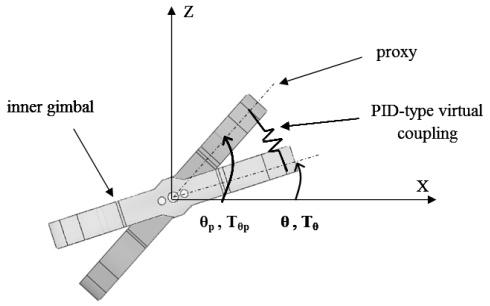

Fig. 4. Principle of PBSMC.

The error dynamics of the proxy is chosen to decay to zero based on a positive rate constant λ towards the sliding surface and is determined by

$$\dot{q}_e + \frac{1}{\lambda}q_e = 0 \quad (9)$$

where

$$q_d - q_p = q_e. \quad (10)$$

On the other hand, torque T_θ is produced by the PID-type virtual coupling in a conventional way:

$$T_\theta = K_p(q_p - q) + K_d(\dot{q}_p - \dot{q}) + K_i\int(q_p - q)dt \quad (11)$$

where K_p, K_d and K_i are positive real numbers, which represent the proportional, derivative and integral gains, respectively. These parameters should be chosen appropriately so that the position of the inner gimbal *q* is

ISBN: 978-988-18210-9-6
ISSN: 2078-0958 (Print); ISSN: 2078-0966 (Online)

controlled to follow the desired position of the proxy q_p in an accurate way.

If inertia of the proxy is I_p, then the equation of the motion of the proxy is given by

$$I_p \ddot{q}_p = T_{\theta p} - T_\theta. \tag{12}$$

Similar to [18, 19], the inertia of the proxy is set to zero to simulate the controller. Therefore, by introducing

$$\eta = \int (q_p - q) dt \tag{13}$$

and using (7), (8) ,(11) and (12), the following set of equations representing the continuous-time state-space of PBSMC is obtained:

$$T = K_p \dot{\eta} + K_d \ddot{\eta} + K_i \eta \tag{14a}$$

$$K_p \dot{\eta} + K_d \ddot{\eta} + K_i \eta - U \,\mathrm{sgn}(S - \dot{\eta} + \lambda \ddot{\eta}) = 0 \tag{14b}$$

$$S = (q_d - q\ ) + \lambda(\dot{q}_d - \dot{q}\ ) \tag{14c}$$

PBSMC is then turned into a digital controller by a discrete time representation of equations 14 using backward difference to approximate derivatives and the value of U at time step k is calculated as:

$$S(k) = (q_d(k) - q\ (k)) + \lambda(\dot{q}_d(k) - \dot{q}\ (k)) \tag{15a}$$

$$U^*(k) = \frac{K_p T + K_d + K_i T^2}{\lambda + T} S(k) + K_i \eta(k-1) + \frac{(K_p + K_i T)\lambda - K_d}{(\lambda + T)T} \Delta\eta(k-1) \tag{15b}$$

$$U(k) = \begin{cases} U^*(k) & if \quad \|U^*(k)\| \le V \\ VU^*(k) / \|U^*(k)\| & if \quad \|U^*(k)\| > V \end{cases} \tag{15c}$$

$$a(k) = \frac{1}{K_p T + K_d + K_i T^2} \{(K_p T + K_d)\eta(k-1) + K_d \Delta\eta(k-1) + T^2 F(k)\} \tag{15d}$$

Here, T is the sampling rate, V is the torque limit and Δ is the backward difference operator.

The advantage of PBSMC over PID and classical sliding mode control is the separation of the dynamics that carry large positional errors, which in the present case is the large amount of change in the desired angle in θ or φ, from the dynamics which responds to small errors between desired and the actual output governed by virtual couplings.

IV. Simulation Results

A. Simulation Environment

The overall simulation model of the gimbaled system is prepared in MATLAB-Simulink® environment, as depicted in Fig. 5. The three main blocks within the simulation environment represent the plant being the two-axis gimbaled platform, the stabilization controller, and the rate sensor.

B. Simulations

In all results of this subsection, the gimbaled platform is excited every 0.04 seconds. Table 1 shows the parameters used in the simulation in accordance with the hardware, so that, unless otherwise noted, the parameter values listed here are used in both the simulations and in the hardware experiments.

1) Set Point Tracking

Here, the behaviors of PID controller and PBSMC under large angular velocity error are compared against desired outputs. The performance of PBSMC and conventional PID controller in elevation and azimuth axes are illustrated in Fig.s 6 and 7, respectively. Fig. 6 also shows the response obtained by classical sliding mode control, in the form given in Eq. (7) with U=20 as a reference. The bold signal in this figure represents the desired tracking command.

For ease of comparison, the gains used in the PBSMC are taken the same as those in the PID controller. The simulation results, given separately in Figs. 6 and 7, indicate in both axes that PID controller has a much larger rise time that creates accumulation error in shorter pulse durations. On the other hand, PBSMC gives more accurate response than the PID controller. In addition, the most important property of PBSMC is that a smooth response, close to a critically damped one, is observed rather than highly overdamped PID responses. PID controller exhibits larger delay in azimuth axis than in elevation, while PBSMC performs swiftly with very low rise time in both axes.

2) Disturbance Rejection

In this part, a sinusoidal angular velocity disturbance with amplitude of 5 deg/s and a frequency of 10 Hz is applied while the desired angular velocity of the elevation axis is zero.

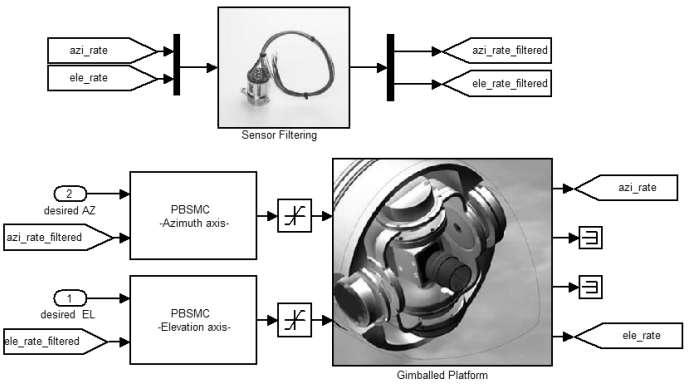

Fig. 5. Simulation model of LOS stabilization system.

Fig. 8 show the comparison in performance between PID and PBSMC stabilization controllers while the inertia of the payload in Y axis (Fig. 8.c and Fig. 8.d), viscous friction on bearings (Fig. 8.b), and the cable stiffness (Fig. 8.a) on the gimbaled platform change. In these figures, the number in the brackets in the legend represents the relevant changing parameter, the multiplier of its original value given in Table I.

TABLE I. Simulation Conditions

Subsystem	Conditions		
Motor + Gimbal	*mass unbalance*	*0.016 m*	
	payload	*0.7 kg*	
	static friction	*0.0004 Nm*	
	coulomb friction	*0.0036*	
	viscous friction	*0.005 Nm/rad/s*	
	cable stiffness	*0.16 Nm/rad*	
Controller	***Azimuth axis***	***PBSMC***	***PID***
	P	*8*	*8*
	I	*0.0435*	*0.0435*
	D	*0.0290*	*0.0290*
	V	*500*	-
	λ	*10*	-
	sample time	*0.00005 s*	*0.00005 s*
Rate Sensor	*bandwidth*	*111 Hz (@ -90° phase*	
	damping ratio	*0.66*	
	noise	*0.0029 °/s/ rt Hz*	

ISBN: 978-988-18210-9-6
ISSN: 2078-0958 (Print); ISSN: 2078-0966 (Online)

Although, increasing the stiffness and the viscous friction deteriorate the performance of both controllers, PBSMC can tolerate these changes at higher levels of angular velocities and the degradation of velocity amplitudes are much less than those for PID, since PID controller accumulates larger errors owing to large delays in large values of rise time.

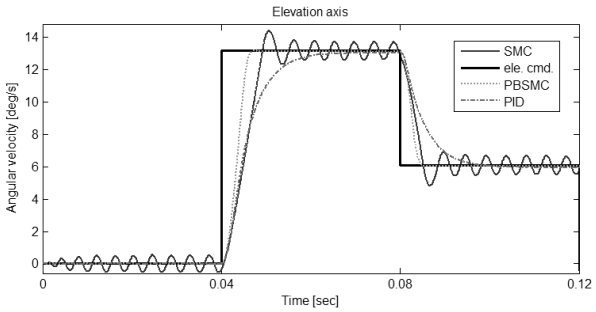

Fig. 6. Closed-loop performance of PBSMC and PID, elevation axis.

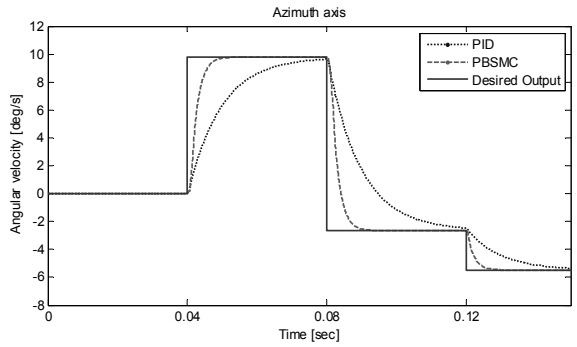

Fig. 7. Closed-loop performance of PBSMC and PID, azimuth axis.

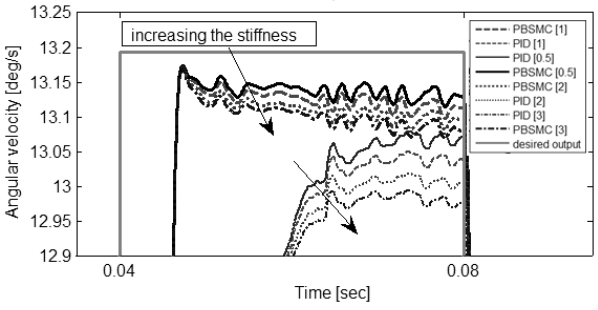

Fig. 8.a Effect of the change in the stiffness to controller responses, elevation axis

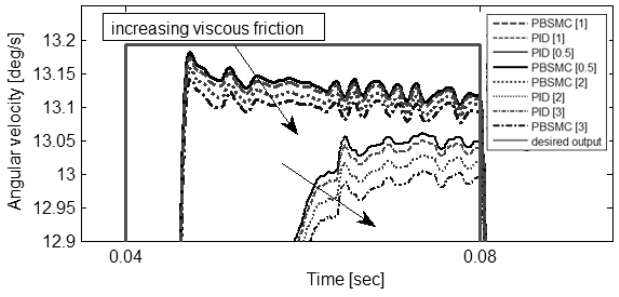

Fig. 8.b Effect of the change in the viscous friction to controller responses.

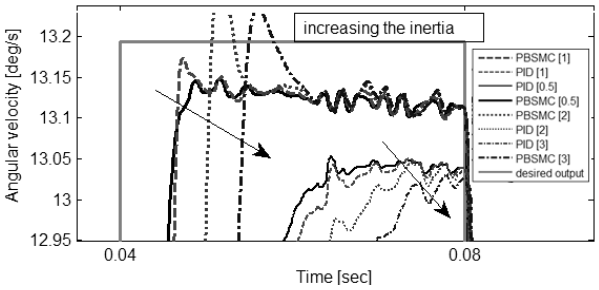

Fig. 8.c Effect of the change in the inertia of the payload in *Y* axis to controller responses.

Comparing all changes in Fig. 8, it can be concluded that highest sensitivity is due to the change in the inertia of the payload in the elevation axis (Fig. 8.b). Changing the inertia of the payload does not affect much the accuracy of the PBSMC, whereas large deterioration in the steady-state settling time of the PID exists. Increasing the inertia further than a certain level (represented as level A, shown by an arrow in Fig. 8.d) results in an overshoot in the response of PBSMC. Since increasing the inertia represents a decrease in the damping ratio in linearized system, gimbaled system becomes an underdamped system resulting in overshoot in the responses of PBSMC. In general, an increase in inertia, when inertia becomes greater than 0.0025 kg-m^2 in our example, leads to deterioration in transient stability which is mainly governed by the damping factor. In addition, a delay due to higher rise time is seen in both controllers if the inertia of the payload is increased.

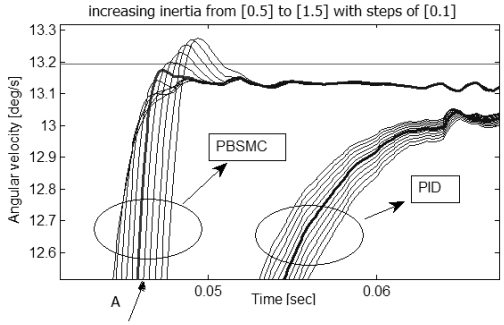

Fig. 8.d Effect of the change in the inertia of the payload in *Y* axis to controller responses, elevation axis

Finally, Fig. 9 shows the control command to the gimbaled platform generated by PID and PBSMC. PBSMC incorporates an optimization based on the proxy coupling and does not generate high-frequency chattering. PID control, on the other hand, cannot generate any optimization without sacrificing its performance.

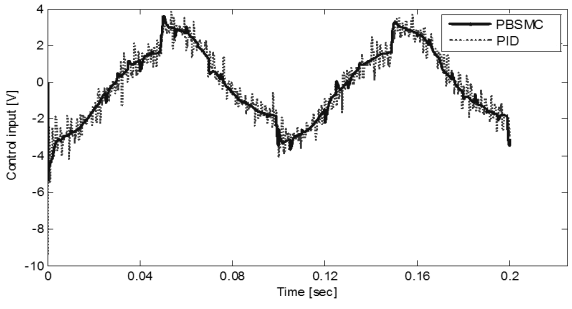

Fig. 9. Control commanded to plant, generated by PID and PBSMC, elevation axis

ISBN: 978-988-18210-9-6
ISSN: 2078-0958 (Print); ISSN: 2078-0966 (Online)

V. Experimental Results

The proposed method is also experimentally tested on the two-axis gimbaled hardware system illustrated in Fig. 1. This experimental setup is controlled using the control law of equation (15). PBSMC and PID controller are both implemented with xPC Target system with a sampling time of 0.05 milliseconds. The angular velocity measurement is taken every millisecond.

Disturbance rejection capability of PBSMC and PID controller in azimuth axis is comparatively assessed. As a disturbance, four sinusoidal angular velocity disturbances are applied with Newport XPS Controller with variable amplitudes and frequencies as listed in Table II.

TABLE II. Given Sinosuidal Disturbances

Case Number	Amplitude (deg/s)	Frequency (Hz)
1	*20*	*10*
2	*20*	*5*
3	*10*	*10*
4	*5*	*10*

Fig. 10 shows that while the amplitude of the disturbance decreases as represented by amplitude values in the brackets in the legend of the figure, amplitude variations in the response of the PBSMC decrease dramatically. In small amplitudes, there are some deviations which are caused by the damping effect in PBSMC. Although, this behavior can be perceived as a drawback when small disturbance exists, this drawback cannot be seen in actual applications. This is because in real-time tests, high disturbance predominantly exists on the gimbaled platform, and the PBSMC can handle this with high precision, which is in contrast to the conventional PID controller equipped with identical gains.

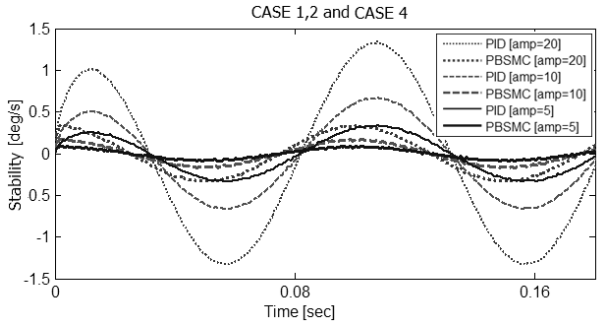

Fig. 10. Experimental results (disturbance rejection)

In addition, Fig. 11 shows the typical tracking error measured in azimuth axis. This result is obtained while 10 deg/s angular rate is given to the plant. It is clear from this figure that the tracking error of PBSMC, equipped with identical gains with the ones of the PID controller, decreases drastically faster than for the case of the PID controller.

The gimbaled mechanics is designed so that the geometrical center of the payload coincides with the intersection of the gimbal axes. However, in the gimbaled platform, there is a large unbalance because of manufacturing. In addition, the cable connection is not perfect. Although, these consequences lead to unpredictable disturbance sources in experiments on hardware, PBSMC still has outperformed PID control and provided robust stabilization.

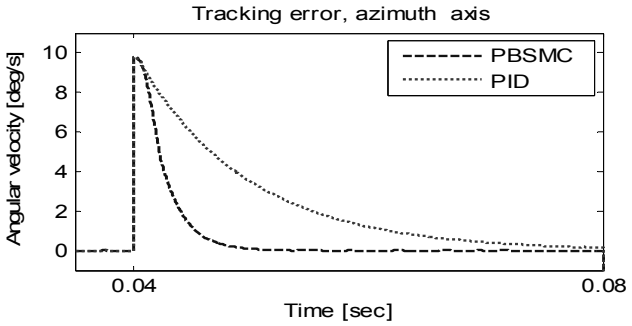

Fig. 11. Tracking error measured in azimuth axis

As a result of experiments run with equal gains for PID and PBSMC, we decided to compare our proposed approach with perfectly tuned PID's. Figs. 12 and 13 show the set point tracking performance and disturbance rejection capability of both controllers: PBSMC and tuned PID, respectively.

Although, the rise time and steady state accuracy of the PID controller has been greatly improved, PBSMC is still found to be superior to tuned PID in both tracking performance and disturbance rejection capability. This is why the PBSMC has been permanently adopted for stabilization in our experimental setup.

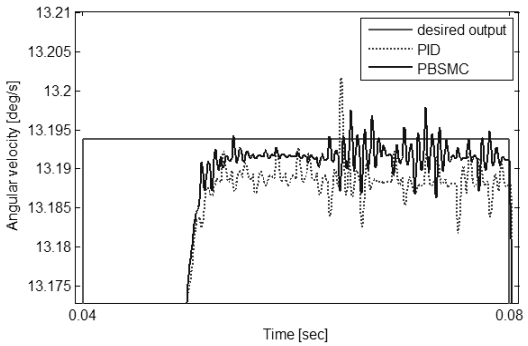

Fig. 12 Simulation result of the performance of PBSMC and PID with *K=200 I=2 D=0.2 F=500000 and λ=2*, elevation axis.

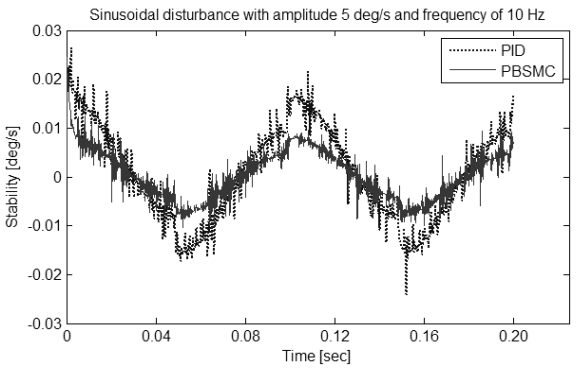

Fig. 13 Simulation results (disturbance rejection) of PBSMC and PID with *K=200 I=2 D=0.2 F=500000 and λ=2*, elevation axis.

VI. Conclusions

This paper describes the PBSMC method developed for the stabilization of a two-axis gimbaled guidance platform. The disturbance rejection capability and tracking

ISBN: 978-988-18210-9-6
ISSN: 2078-0958 (Print); ISSN: 2078-0966 (Online)

performance of PBSMC are found to be far superior to those of PID control.

The missile dynamics and the aerodynamic conditions cannot be precisely estimated. Hence, disturbance on the gimbal base is highly uncertain. Therefore, disturbance handling capability of the PBSMC is now being evaluated through more performance criteria other than variable sinusoidal disturbances at the base of the gimbaled platform. However, our recent real-time experiments on actual missile guidance systems show that the PBSMC can overcome a large range of disturbances with different amplitude patterns while preserving stability.

ACKNOWLEDGMENT

This work was supported by Roketsan Missiles Industries Inc.

REFERENCES

[1] Titterton D., Weston J., “Strapdown Inertial Navigation Technology”, Second Edition.

[2] Smith, B.J.; Schrenk, W.J.; Gass, W.B.; Shtessel, Y.B.; , "Sliding mode control in a two-axis gimbal system," Aerospace Conference, 1999. Proceedings. 1999 IEEE , vol.5, no., pp.457-470 vol.5, 1999.

[3] R. A. Decarlo, S. H. Zak, G. P. Matthews, “Variable Structure Control of Nonlinear Multivariable Systems: A Tutorial”, Proc. IEEE, Vol76, No. 3, pp 212-232, 1988.

[4] Min Sig Kang, Joon Lyou, Jong Kwang Lee, “Sliding mode control for an active magnetic bearing system subject to base motion”, Mechatronics, Volume 20, Issue 1, Special Issue on 'Servo Control for Data Storage and Precision Systems', 17th IFAC World Congress 2008.

[5] Carl Knospe, “PID Control”, IEEE Control Systems Magazine, pp. 30-32, February 2006.

[6] Ki-Jun Seong; Ho-Gyun Kang; Bo-Yeon Yeo; Ho-Pyeong Lee; , "The Stabilization Loop Design for a Two-Axis Gimbal System Using LQG/LTR Controller," SICE-ICASE, 2006. International Joint Conference , vol., no., pp.755-759, 18-21 Oct. 2006.

[7] Yonggen Han; Yanhong Lu; Haitao Qiu; , "An Improved Control Scheme of Gyro Stabilization Electro-Optical Platform," Control and Automation, 2007. ICCA 2007. IEEE International Conference on , vol., no., pp.346-351, May 30 2007-June 1 2007.

[8] Wei Ji; Qi Li; Bo Xu; Jun-Jun Tu; De-An Zhao; , "Cascade servo control for LOS stabilization of opto-electronic tracking platform—design and self-tuning," Information and Automation, 2009. ICIA '09. International Conference on , vol., no., pp.1034-1039, 22-24 June 2009.

[9] Stein, G.; Athans, M.; , "The LQG/LTR procedure for multivariable feedback control design," Automatic Control, IEEE Transactions on , vol.32, no.2, pp. 105- 114, Feb 1987.

[10] Ray, L.R.; , "Stability robustness of uncertain LQG/LTR systems," Automatic Control, IEEE Transactions on , vol.38, no.2, pp.304-308, Feb 1993.

[11] Abdullah I. Al-Odienat, Ayman A. Al-Lawama, “The Advantages of PID Fuzzy Controllers over the Conventional Types”, American Journal of Applied Sciences 5 (6): 653-658, 2008.

[12] Nie, J.; , "Fuzzy control of multivariable nonlinear servomechanisms with explicit decoupling scheme," Fuzzy Systems, IEEE Transactions on , vol.5, no.2, pp.304-311, May 1997.

[13] Williams, R.J., Zipser, D. “Experimental analysis of the real-time recurrent learning algorithm”, Connection Science, vol.1, no. 1, pp. 87–111, 1989.

[14] Xiang, Z.; Bi, G.; , "Mixed gradient based fast learning algorithm for MLP with its applications to MQAM digital mobile radio receptions,"Acoustics, Speech, and Signal Processing, 1993. ICASSP-93., 1993 IEEE International Conference on , vol.1, no., pp.473-476 vol.1, 27-30 April 1993.

[15] Giles, C.L.; Dong Chen; Guo-Zheng Sun; Hsing-Hen Chen; Yee-Chung Lee; Goudreau, M.W.; , "Constructive learning of recurrent neural networks: limitations of recurrent cascade correlation and a simple solution," Neural Networks, IEEE Transactions on , vol.6, no.4, pp.829-836, Jul 1995.

[16] Utkin, V.I., 1978. “Sliding Modes and their Application in Variable Structure Systems”, MIR Publishers, Moscow, pp: 9-38.

[17] Fujisawa, S. and K. Kawada, 2004. Speed Control of 3- mass System with Sliding mode control and CMAC. Proceeding of the IEEE Conference on Systems, Man and Cybernetics, Oct. 10-13, IEEE Xplore Press, USA, pp: 4400- 4407.

[18] Kikuuwe, R.; Fujimoto, H.; , "Proxy-based sliding mode control for accurate and safe position control," Robotics and Automation, 2006. ICRA 2006. Proceedings 2006 IEEE International Conference on , vol., no., pp.25-30, 15-19 May 2006.

[19] Kikuuwe, R.; Yamamoto, T.; Fujimoto, H.; , "Low-Force Kinesthetic Guidance for Accurate Positioning and Tracking," Haptic Interfaces for Virtual Environment and Teleoperator Systems, 2006 14th Symposium on , vol., no., pp. 491- 498, 25-26 March 2006.

[20] M. Van Damme, B. Vanderborght, B. Verrelst, R. Van Ham, F. Daerden, and D. Lefeber, “Proxy-based sliding mode control of a planar pneumatic manipulator,” *Int. J. Robot. Res.*, vol. 28, no. 2, pp. 266–284, 2009.

[21] Guanglin Li, Fuming Sun, Na Cheng, "Performance Analysis of UKF for Nonlinear Problems," iita, vol. 2, pp.209-212, 2009 Third International Symposium on Intelligent Information Technology Application, 2009.

[22] K. Xiong, H. Y. Zhang, and C. W. Chan, “Performance evaluation of UKF-based nonlinear filtering,” Automatica, vol.42, pp.261-270,2006.

[23] Simo Särkkä, “Sigma Point and Particle Approximations of Stochastic Differential Equations in Optimal Filtering” Helsinki University of Technology , Nalco Company, May, 2008.

[24] L. Meirovitch. “Methods of Analytical Dynamics.” McGraw-Hill, New York, NY, 1970.

[25] Dejun Sheng; Dapeng Fan; Hu Luo; Xutao Nie; , "Bond Graph Approach to the Modeling and Simulation of a Two-Axis Pointing and Tracking System," Mechatronics and Automation, 2007. ICMA 2007. International Conference on , vol., no., pp.2337-2341, 5-8 Aug. 2007.